Published by Avanti Publishers

Global Journal of Earth Science and Engineering

ISSN (online): 2409-5710

Age and Geochemical Characteristics of Nansu Rapakivi Granite in Jiaobei Uplift Belt, Qingdao

Feng Qiao, Sheng Rongtian*, Li Xuewei, Dai Ruiwen and Jiang Yong

School of Earth Science and Engineering, Shandong University of Science and Technology, Qingdao, Shandong 266590, China

ARTICLE INFO

Article Type: Research Article

Keywords:
Partial melting
Rapakivi granite
Zircon U-Pb age
Early Cretaceous
Geochemical characteristics

Timeline:
Received: February 25, 2022
Accepted: April 28, 2022
Published: May 10, 2022

Citation: Qiao F, Rongtian S, Xuewei L, Ruiwen D, Yong J. Age and Geochemical Characteristics of Nansu Rapakivi Granite in Jiaobei Uplift Belt, Qingdao. Glob J Earth Sci Eng. 2022; 9: 51-64.

DOI: https://doi.org/10.15377/2409-5710.2022.09.4

ABSTRACT

LA-ICP-MS zircon U-Pb geochronology from Nansu large Rapakivi granite in the Jiaobei uplift belt shows the concordant age is 116.5±0.32Ma and the weighted average age is 116.7±0.89Ma, belonging to the late Yanshanian products of Early Cretaceous. The rock geochemical characteristics show that the SiO_2 content of rapakivi granite ranges from 70.30% to 71.65%, with an average of 70.975%, A / CNK is 0.871 ~ 0.895 (average 0.883). K_2O content is 4.70 ~ 5.75%, with an average of 5.14%, which is characterized by high potassium. Regarding trace elemental patterns, all the studied samples are enriched in large — ion-lithophile elements, e.g., K and Rb, and depleted in high-field-strength elements, e.g., Nb, Ta, and Ti. In terms of the chondrite-normalized rare earth element patterns, the Nansu samples are characterized by the strong enrichment of light rare earth elements (LREE) compared with heavy rare earth elements (HREE) and the absence of negative Eu anomalies. The Nansu ring porphyry granite is of high Sr and low Yb type, belonging to type I adakite, and formed in a high-pressure medium high-temperature environment of about 23km at depth and about 670°C. It is speculated that it was formed in the island arc environment and is related to the subduction of the Mesozoic Pacific plate.

*Corresponding Author
Email: 547168422@qq.com
Tel: 17854259184

1. Introduction

A large number of Yanshanian granites are developed in Jiaodong Peninsula to the East of the Tanlu fault zone, which is closely related to the giant Jiaodong polymetallic nonferrous deposit [1-4]. Therefore, it is very important to study the genesis of granites in this period [5-10]. Previous studies on the genesis of rapakivi granite have many disputes, such as exsolution, metasomatism, changes in pressure and water content during magma rise, magma mixing and assimilation and contamination, etc. [11-18]. However, there are commonalities in the understanding of its formation environment. Most studies show that it occurs in the stable Craton and its marginal fault zone and is the product of late orogeny [19-24]. Taking Nansu Rapakivi granite as an example, this paper discusses the differential crystallization process and formation history of Nansu Rapakivi granite through the study of outcrop detailed mineral crystal formation sequence and rock types, combined with single-grain zircon U-Pb chronology and geochemistry.

2. Materials and Methods

2.1. Materials

The major elements are mainly determined by wavelength dispersive X-ray fluorescence spectrometer, and the trace elements are determined by plasma mass spectrometer. The main and trace elements of the whole rock were determined on 8 samples of Nansucun Rapakivi granite. The determination results are shown in Table **1**. The selected samples were ground, selected, and made into target samples. U-Pb isotope analysis was carried out on a laser-plasma mass spectrometer (LA-ICP-MS). The test data are shown in Table **2**.

2.2. Methods

The exposed area of Nansu large-scale rapakivi granite (N37°8'37", E120°7'44") in Laizhou City, Yantai, Jiaodong is very fresh due to the mining of building stone outcrops, and the rock samples are hardly affected by weathering. When collecting geochemical and chronological samples, try to avoid developing parts such as xenoliths and calcite veins. A total of 8 geochemical samples and 5kg chronological samples were collected.

The major elements are mainly determined by wavelength dispersive X-ray fluorescence spectrometer. The instrument model is ARL advent XP + wavelength dispersive X-ray fluorescence spectrometer, and the detection basis is GB / t1450628-2010 silicate rock chemical analysis method (Part 28: Determination of 16 primary and secondary components GB / t14506.14-2010 silicate rock chemical analysis method) and ferrous oxide content (Part 14). The results are shown in Table **1**. Trace elements are analyzed by plasma mass spectrometer with an accuracy of 0.3 ~ 0.9%, as shown in Table **2**.

The selection and target making of zircon were completed in the rock and mineral Laboratory of Langfang China Railway geophysical prospecting and exploration Co., Ltd., and the cathodoluminescence photography of zircon was completed in Langfang Tuoxuan Rock and Mineral Testing Service Co., Ltd. with Fei quanta 450 (equipped with mono CL4) scanning electron microscope. Zircon separation adopts the heavy sand analysis method. The basic instruments are a binocular microscope and magnetic separator. The basic separation operation procedures are screening coarse panning (ensure that the particle size is greater than > 0.05mm), strong magnetic separation, electromagnetic separation, fine panning, packaging, and mineral separation. When selecting, it is required not to distinguish the color, particle size, and self shape degree and select all or most of them as far as possible to avoid artificial subjective screening. Zircon particles are randomly selected without classification and fixed with resin to make the sample target. After grinding and polishing, the internal profile of zircon adhered to the sample target can be exposed entirely; The prepared sample target is photographed by reflected light, transmitted light, and cathodoluminescence (CL) to obtain the crystal morphology and internal structure information of zircon, so as to select an appropriate area for U-Pb isotope determination.

Table 1: Major (wt%) and trace elements of Nansu rapakivi granite (×10^{-6}) statistical table.

Sample	NS-01	NS-02	NS-03	NS-04	NS-05	NS-06	NS-07	NS-08
SiO_2	71.16	70.92	70.66	71.08	70.95	71.65	70.30	70.63
Al_2O_3	13.81	13.98	13.86	13.58	13.98	13.56	13.94	13.61
TFe_2O_3	2.03	1.92	2.12	2.18	1.98	1.87	2.01	2.19
MgO	0.75	0.68	0.84	0.88	0.76	0.72	0.802	0.887
CaO	1.91	1.64	2.11	2.10	1.87	1.83	1.91	2.08
Na_2O	4.05	3.89	4.14	4.05	4.00	3.89	3.98	3.97
K_2O	5.06	5.75	4.79	4.70	5.22	5.29	5.41	4.87
MnO	0.040	0.037	0.035	0.042	0.036	0.035	0.032	0.036
TiO_2	0.264	0.248	0.278	0.291	0.267	0.242	0.259	0.289
P_2O_5	0.129	0.125	0.144	0.149	0.128	0.129	0.137	0.154
LOI	0.573	0.558	0.772	0.689	0.569	0.534	0.948	1.00
FeO	1.09	1.03	1.13	1.23	1.13	1.03	1.11	1.13
A/CNK	0.883	0.895	0.875	0.871	0.893	0.876	0.876	0.871
Y	9.26	9.16	9.97	10.4	9.51	9.07	9.40	10.7
La	48.2	51.3	55.4	67.9	59.2	62.4	63.1	61.9
Ce	84.0	88.1	95.4	112	98.4	102	103	106
Pr	9.28	9.58	10.5	12.0	10.5	10.5	10.9	11.6
Nd	30.7	31.2	34.4	38.0	33.8	33.0	34.7	38.0
Sm	4.53	4.61	5.04	5.49	4.79	4.62	4.88	5.59
Eu	1.53	1.62	1.66	1.64	1.63	1.59	1.76	1.92
Gd	4.26	4.38	4.85	5.27	4.78	4.72	4.91	5.32
Tb	0.47	0.47	0.53	0.57	0.50	0.48	0.51	0.57
Dy	1.84	1.84	2.04	2.13	1.91	1.81	1.95	2.21
Ho	0.32	0.32	0.35	0.37	0.33	0.32	0.33	0.38
Er	1.14	1.10	1.19	1.14	1.16	1.13	1.19	1.36
Tm	0.15	0.15	0.16	0.16	0.15	0.15	0.15	0.16
Yb	0.94	0.93	0.98	1.03	0.96	0.93	0.92	1.03
Lu	0.15	0.15	0.17	0.16	0.16	0.15	0.15	0.16
Sc	6.60	6.45	7.28	9.29	6.54	6.90	6.82	7.08
V	23.5	22.0	25.4	26.3	23.3	22.4	24.2	27.7
Cr	18.3	14.0	16.1	14.9	13.5	14.5	16.2	15.6
Co	3.74	3.41	4.08	3.99	3.71	3.43	3.81	4.31
Ni	7.47	5.54	7.03	6.59	6.07	5.80	6.47	6.80
Cu	4.04	4.24	4.24	4.45	4.70	3.97	4.15	5.03
Zn	35.3	34.4	29.0	31.5	31.8	32.0	25.4	26.0
Ga	19.2	18.7	19.9	19.1	19.4	19.3	19.2	19.1
Rb	167	183	151	148	172	188	165	147
Sr	566	535	628	610	594	581	657	685
Zr	99.5	89.3	94.0	106	91.8	94.9	86.7	89.5
Nb	14.3	13.9	15.1	14.4	15.0	13.8	14.2	14.4
Ba	1528	1792	1581	1490	1607	1703	1918	1996
Hf	3.61	3.25	3.49	3.62	3.45	3.57	3.14	3.21
Ta	1.07	1.06	1.17	1.29	1.12	1.07	1.03	1.09

Pb	25.8	28.1	23.0	19.7	23.4	25.9	23.0	21.1
Th	25.1	26.9	23.3	25.4	25.9	27.9	23.0	17.6
U	2.50	2.45	4.28	4.15	4.67	3.12	3.45	2.85
∑REE	187.55	195.78	212.58	247.80	218.25	223.25	228.39	235.68
La/Nb	3.36	3.69	3.67	4.72	3.94	4.53	4.45	4.30
Th/La	0.52	0.53	0.42	0.37	0.44	0.45	0.36	0.28
Zr/Hf	27.58	27.49	26.91	29.12	26.59	26.57	27.58	27.87
Zr/Y	10.74	9.75	9.43	10.16	9.66	10.47	9.22	8.36
Sr/Yb	602.99	576.19	640.06	593.48	621.88	622.40	711.38	666.15
(La/Yb)n	34.89	37.55	38.38	44.84	42.09	45.40	46.43	40.88
(La/Sm)n	6.65	6.95	6.87	7.71	7.72	8.44	8.08	6.91

Table 2: Statistics of zircon LA-ICP-MS U-Pb ages of Nansu rapakivi granite.

Point Number	Th	U	Th/U	$^{207}Pb/^{206}Pb$		$^{207}Pb/^{235}U$		$^{206}Pb/^{238}U$		$^{207}Pb/^{206}Pb$		$^{207}Pb/^{235}U$		$^{206}Pb/^{238}U$	
	($\times10^{-6}$)			Ratio	1σ	Ratio	1σ	Ratio	1σ	Age (MA)	1σ	Age (MA)	1σ	Age (MA)	1σ
NS-01	263.34	264.82	0.99	0.05019	0.00331	0.13286	0.00828	0.0192	0.00033	203.8	146.08	126.7	7.42	122.6	2.1
NS-02	210.18	302.42	0.69	0.04947	0.00244	0.12625	0.00572	0.01851	0.00026	170.2	111.14	120.7	5.16	118.2	1.66
NS-03	327.68	321.94	1.02	0.04984	0.0024	0.12653	0.00557	0.01841	0.00026	187.8	108.2	121	5.02	117.6	1.64
NS-04	286.16	232.33	1.23	0.04802	0.00342	0.12116	0.00822	0.0183	0.00032	99.2	161.5	116.1	7.44	116.9	2.04
NS-05	401.17	380.55	1.05	0.0507	0.00251	0.13203	0.006	0.01889	0.00027	227	110.42	125.9	5.38	120.6	1.72
NS-06	332.95	279.24	1.19	0.05089	0.00184	0.12547	0.00392	0.01788	0.00022	235.7	81.42	120	3.54	114.3	1.41
NS-07	242.51	291.48	0.83	0.04896	0.00248	0.12549	0.00588	0.01859	0.00027	146	114.84	120	5.31	118.7	1.68
NS-08	395.62	361.36	1.09	0.04876	0.00269	0.11984	0.00615	0.01782	0.00027	136.5	124.58	114.9	5.58	113.9	1.71
NS-09	221.51	202.95	1.09	0.04861	0.00325	0.12395	0.00788	0.01849	0.00031	128.8	150.37	118.6	7.12	118.1	1.96
NS-10	436.15	293.19	1.49	0.05003	0.0026	0.12495	0.00601	0.01811	0.00026	196.3	116.41	119.5	5.43	115.7	1.67
NS-11	327.54	352.74	0.93	0.05007	0.00294	0.12918	0.00711	0.01871	0.0003	198.3	131.07	123.4	6.4	119.5	1.9
NS-13	244.82	256.48	0.95	0.0503	0.00272	0.12487	0.0063	0.018	0.00026	209	120.8	119.5	5.68	115	1.67
NS-15	205.22	275.04	0.75	0.04968	0.00307	0.12607	0.00734	0.0184	0.00029	180	137.77	120.6	6.61	117.6	1.87
NS-16	242.13	257.85	0.94	0.04982	0.00325	0.12607	0.00778	0.01835	0.00031	186.7	144.97	120.6	7.01	117.2	1.94
NS-18	324.55	338.37	0.96	0.04974	0.0026	0.12524	0.00605	0.01826	0.00027	182.9	117.21	119.8	5.46	116.6	1.71
NS-20	328.39	337.57	0.97	0.04979	0.00236	0.12352	0.00536	0.01799	0.00025	185.1	106.74	118.3	4.84	114.9	1.58
NS-21	287.72	269.73	1.07	0.04858	0.00252	0.12175	0.00586	0.01817	0.00026	127.8	117.84	116.7	5.3	116.1	1.67
NS-22	199.49	166.95	1.19	0.04955	0.00371	0.1264	0.00904	0.0185	0.00034	174	165.98	120.9	8.15	118.2	2.15
NS-23	201.86	206.66	0.98	0.04706	0.00291	0.11989	0.00701	0.01847	0.00028	52.1	141.65	115	6.36	118	1.8
NS-24	322.57	240.33	1.34	0.0485	0.00353	0.11923	0.00828	0.01783	0.00031	123.7	162.85	114.4	7.51	113.9	1.97
NS-25	274.32	304.14	0.90	0.0489	0.00257	0.1199	0.00585	0.01778	0.00026	143.2	118.99	115	5.3	113.6	1.66
NS-26	280.77	236.97	1.18	0.05006	0.00337	0.12715	0.00812	0.01842	0.00032	197.6	149.31	121.5	7.32	117.7	2
NS-27	233.38	285.21	0.82	0.04875	0.00252	0.11959	0.00574	0.01779	0.00025	136	117.35	114.7	5.21	113.7	1.61
NS-29	367.22	263.92	1.39	0.04949	0.00314	0.12349	0.0074	0.0181	0.0003	170.9	141.87	118.2	6.69	115.6	1.91
NS-32	269.9	267.66	1.01	0.04855	0.00256	0.12167	0.00596	0.01817	0.00026	126.2	119.53	116.6	5.39	116.1	1.66
NS-33	311.11	255.31	1.22	0.04931	0.00396	0.12655	0.00972	0.01861	0.00036	162.4	177.48	121	8.76	118.9	2.3
NS-34	278.47	296.46	0.94	0.04871	0.00241	0.12782	0.00583	0.01903	0.00027	134.1	112.38	122.1	5.25	121.5	1.69

Zircon U-Pb dating was completed in the State Key Laboratory of continental dynamics, Northwestern University. U-Pb isotope analysis was carried out on a laser-plasma mass spectrometer (LA-ICP-MS). The laser ablation system is a geolas200m laser (working substance are f-excimer with a wavelength of 193nm) produced by lambda Physik company in Germany, with helium as carrier gas and spot beam aperture of 20μm. Denudation depth 20 ~ 40μm. The laser frequency is 10Hz, and the energy is 0.032 ~ 0.036J. The isotopic composition is corrected by external standard with standard sample 91500. The specific analysis method of LA-ICP-MS is shown in the literature [26, 27].

3. Regional Geological Background

The study area is located in Nansu village, Laizhou City, and Yantai City. It is a large-scale rapakivi granite, which is located in the Jiaobei uplift zone (Fig. **1**). Jiaobei area is located in the East of the North China plate. To the East is the famous Sulu UHP metamorphic belt. Bounded by the Tanlu fault zone and Wulian Rongcheng fault zone, large-scale Mesozoic granites are developed in the Jiaobei uplift zone, including many large-scale rapakivi granites. In the Mesozoic, affected by the SE-NW compression of the paleo Pacific plate, the Jiaodong area developed multi-stage strong tectonic activities and active deep and shallow magmatism, especially the Mesozoic magmatism, which had a vital impact on the geological structure, tectonic evolution, diagenesis and mineralization of Jiaobei terrane since the Mesozoic.

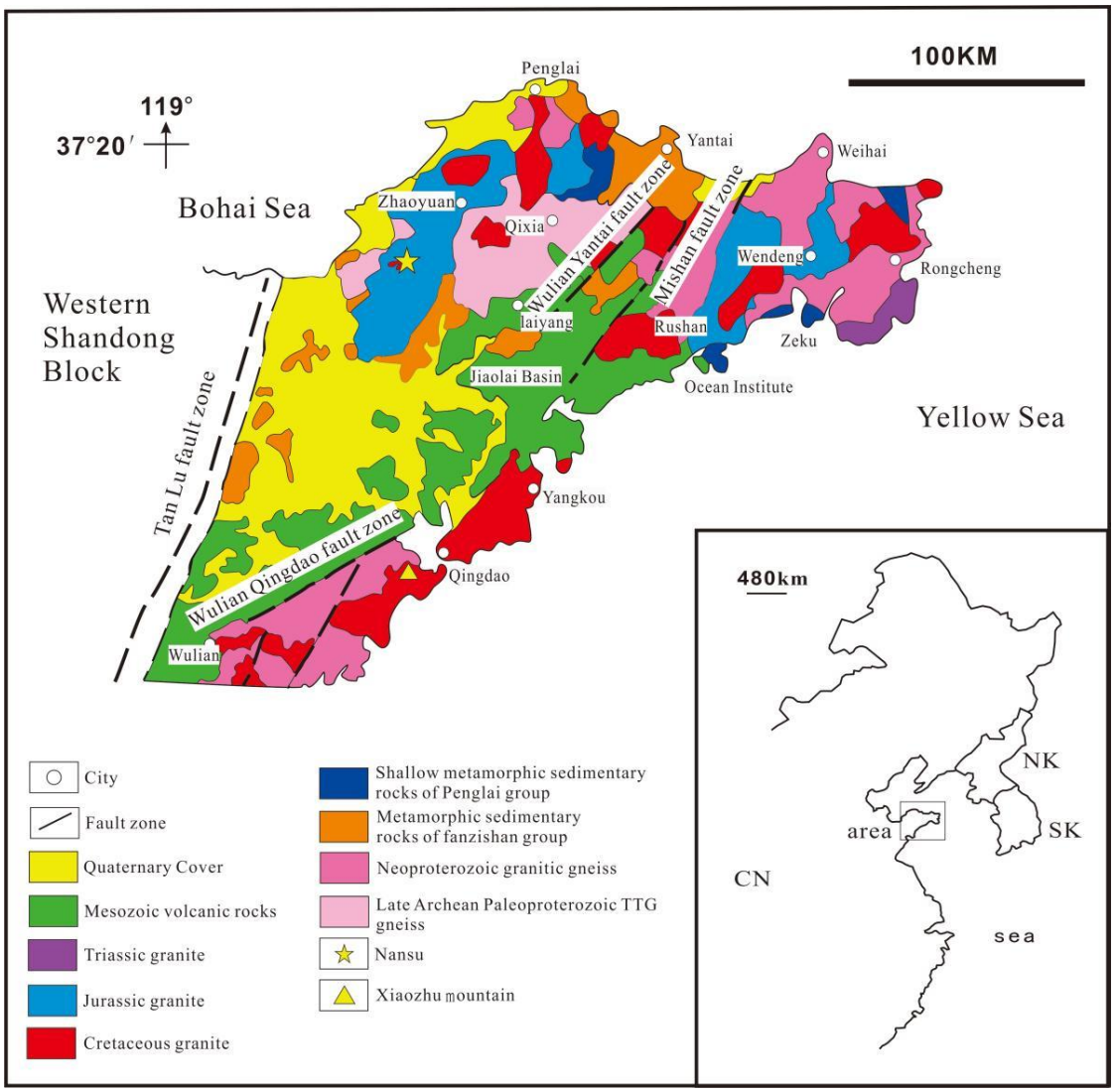

Figure 1: Geological Sketch of Jiaodong area where Nansu rapakivi granite body is located.

4. Petrology of Nansu Rapakivi Granite

A large area of exposed acid granite was developed in the early Cretaceous in the Jiaodong area [25], which contains a large number of rapakivi granite bodies, and Nansu Rapakivi granite is one of its typical representatives. Nansu ring porphyry granite is a medium coarse-grained K-feldspar granite with massive structure and porphyritic structure and rich ring porphyritic phenocrysts. The ringspot is a special structure with ovoid flesh red and light red potassium feldspar, and some are surrounded by light gray white plagioclase shells (Fig. **2**). It is unevenly distributed, and some are linearly developed. About 20% ~ 30% of potassium feldspar, 15% ~ 20% of plagioclase, and 35% of quartz are found in the rapakivi granite. Accessory minerals include biotite, amphibole, sphene, etc. Potassium feldspar has coarse particles, the crystal form is euhedral semi heteromorphic, the particle size is 0.8 ~ 2.5cm, it is plate-shaped oval, the surface is kaolinized, it has an obvious ring structure, the center is gray-black, the outer ring is flesh red, and some are surrounded by albite. Plagioclase is mostly light grayish-white, having the shape of a heteromorphic-subhedral plate. Quartz is smoke gray, granular and mostly filled between feldspar particles (Fig. **2**).

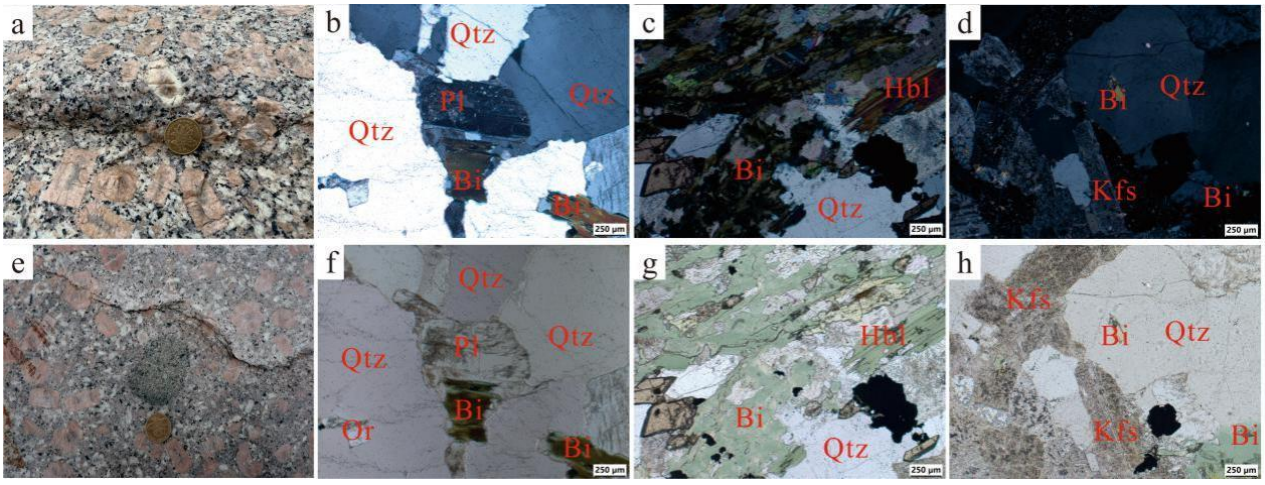

a: plagioclase porphyry with albite crust, partially developed albite crust; b, c, d: orthogonal polarization; e: diorite xenoliths in rapakivi granite; f, g, h: single polarized light; Bi-biotite; Qtz - quartz; Pl-plagioclase; Kfs-potassium feldspar; Hbl-amphibole

Figure 2: Photos and micrographs of field rock outcrop of Nansu granite.

5. Test Result

5.1. Characteristics of Major and Trace Elements

5.1.1. Principal Element

The SiO_2 content of Nansu Rapakivi granite is 70.30% ~ 71.65%, with an average of 70.92%; K_2O + Na_2O content is 8.75% ~ 9.64%, with an average of 9.13%; K_2O / Na_2O = 1.16 ~ 1.48, with an average of 1.12; K_2O content is 4.70% ~ 5.75%, with an average of 5.14%. K_2O content is high; Al_2O_3 content is 13.56% ~ 13.98%, with an average of 13.79%, A/ CNK is 0.871 ~ 0.895, with an average of 0.883, which is quasi aluminum. The content of MgO is 0.72% ~ 0.887%, with an average of 0.79%. The content of CaO is 1.64% ~ 2.08%, with an average of 1.93%. The content of TiO_2 is 0.242 ~ 0.289%, with an average of 0.27%. In Nansu Rapakivi granite, the contents of CaO, MgO, and TiO_2 are low. A / CNK-A / NK, SiO_2- K_2O, SiO_2- K_2O + K_2O rock type combination map shows that Nansu large-scale rapakivi granite belongs to quasi aluminous shoshonite and high potassium series [28], which is in the transitional area of alkaline and sub-alkaline (Fig. **4**).

5.1.2. Trace Element

The total REE contentΣREE of Nansu large-scale Rapakivi granite is 187.55×10^{-6} ~ 247.80×10^{-6}μg/g, with an average of 218.66×10^{-6}μg/g. The REE distribution mode is three-stage (Fig. **4**). The slope of the light REE curve is

steep, the heavy REE is flat, and the fractionation is poor, indicating that it is a crustal melting product belonging to a relatively gentle REE distribution mode [29]. The (La/Sm)n ratio is between 6.20 and 8.08, which is p-type (enrichment type) and LREE enrichment. Yb content is 0.92×10^{-6} ~ 1.03×10^{-6}μg/g, (La/Yb)n is 34.89 ~ 46.43μg/g, Eu shows slight negative anomaly, and Nb and. Ti shows an obvious negative anomaly. Nansu large-scale rapakivi granite belongs to a relatively gentle REE distribution model, with light REE enrichment and heavy REE loss.

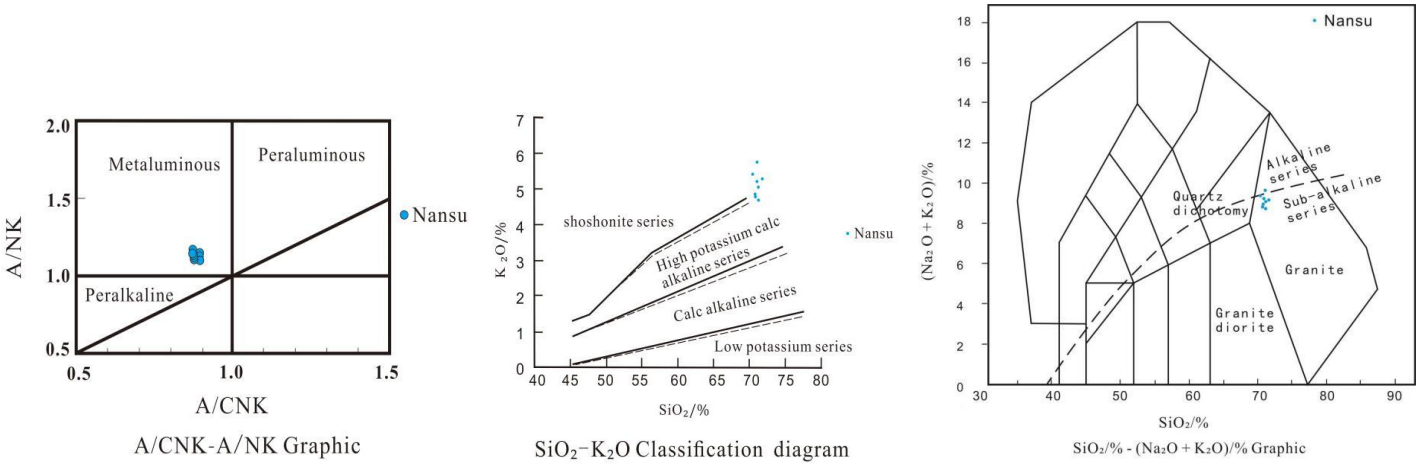

Figure 3: Rock-type combination of Nansu granite.

The spider net diagram of trace elements in the primitive mantle is consistent with the rare earth element distribution pattern diagram of chondrite (Fig. **4** and Fig. **5**), showing that Nb, Ce, Zr, Eu, and Ti are negative anomalies and Pb is positive anomalies. Sr content is 535 ~ 685×10^{-6}μg/g, an average of 607×10^{-6}μg/g; Yb is 0.93 ~ 1.03×10^{-6}μg/g, with an average of 0.96×10^{-6}μg/g, characterized by high Sr and low Yb.

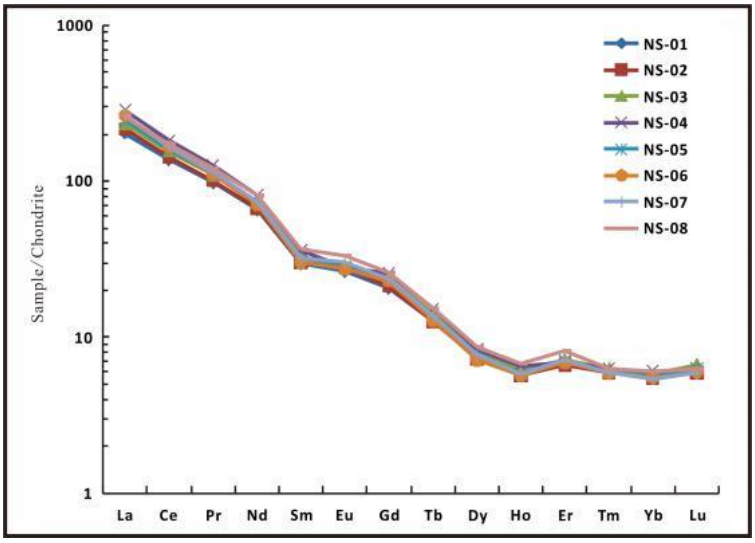

Figure 4: REE distribution pattern of Nansu Rapakivi granite (original mantle standardization data is quoted from the literature [30]).

5.2. Zircon U-Pb Age

35 single grain zircons were selected from Nansu ring porphyry granite samples for U-Pb dating by la-icp-ms. 27 valid data were obtained from 35 zircons. Most of the zircons in the sample are hexagonal short columnar, and the rest are irregular granular, colorless and transparent, self-shaped to semi self-shaped. The length and diameter of zircon are about 80 ~ 140 μm. The length-width ratio is 1.2:1 ~ 2.2:1, the edges and corners are

relatively clear, and the closely developed magmatic rhythmic concussion ring is magmatic crystalline zircon (Fig. **6**). The Th content of 27 zircons is 199.45 × 10^{-6} ~ 436.15 × 10^{-6} μg/g, u content is 166.95 × 10^{-6} ~ 380.55 × 10^{-6} μg/g, Th / U values are between 0.75 and 1.49 (Table **2**), which is in line with the standard that the ratio of magmatic zircon to zircon is greater than 0.4. The concordant age of 27 single grain zircons is 116.5 ± 0.32Ma, and the weighted average age is 116.7 ± 0.89Ma (Fig. **7**). They have very good consistency, representing the crystallization age of Nansu large-scale rapakivi granite, which was formed in the early Cretaceous.

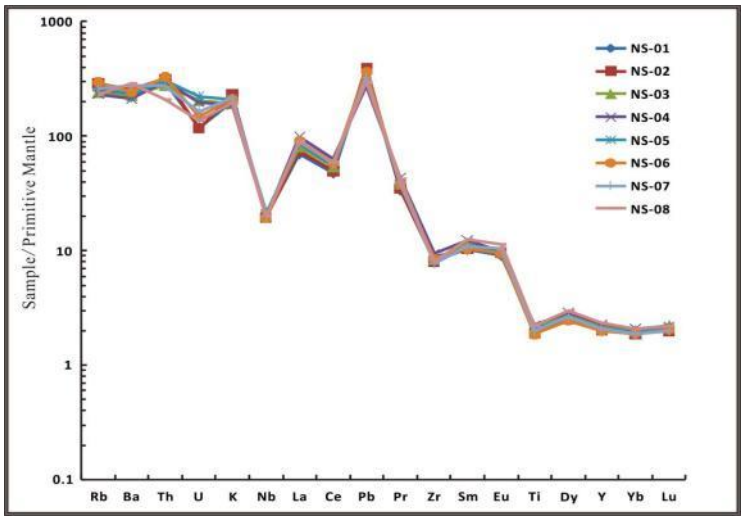

Figure 5: Trace element spider diagram of Nansu Rapakivi granite (chondrite standardization data is quoted from the literature [31]).

Figure 6: Cathodoluminescence diagram of representative zircon and corresponding age data of nansu rapakivi granite.

6. Discussion

6.1. Magmatic Crystallization Differentiation Process

The formation of rapakivi granite has experienced a long evolutionary history, which can be reflected not only in the sequence of mineral crystallization of the rock but also in the length of time used in the growth process of a single mineral.

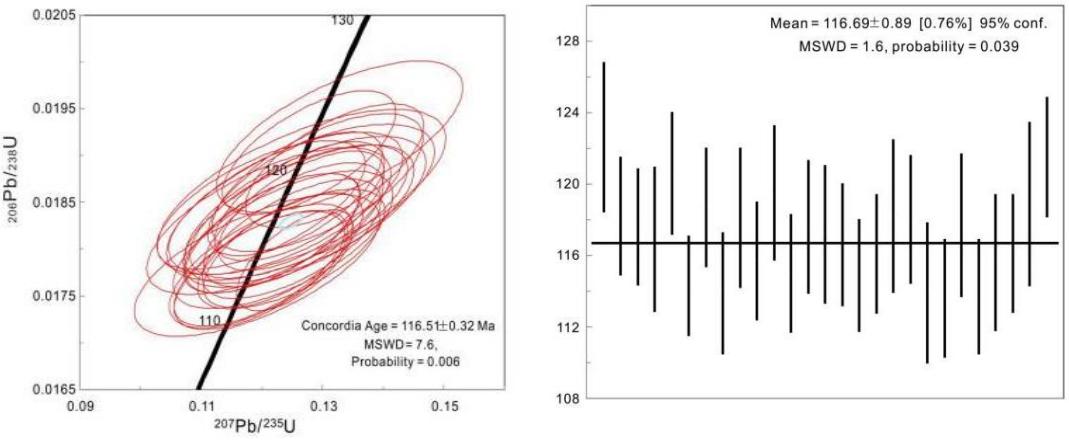

Figure 7: Zircon age concordance and weighted age distribution of Nansu rapakivi granite.

In the process of magmatic evolution, new minerals in the magmatic system continue to crystallize out of the melting system. The general trend of crystallization differentiation is: in the early stage, some minerals are mainly composed of iron and magnesium, such as amphibole, magnetite, pyroxene, and calcline, etc. Over time, in the late stage, quartz, alkali feldspar, and other minerals with high silicon and aluminum content are generally crystallized, and the magma evolves in the direction of silicon-rich, alkali-rich, and iron replacing magnesium. The content of SiO_2 increases relatively with the evolution of magma.

Firstly, according to the automorphic degree, arrangement order, intersecting relationship, symbiotic association relationship, or Bowen reaction sequence of mineral crystals in the outcrop rock of Nansu rapakivi granite, the crystallization order of minerals can be studied so as to roughly determine the growth history of minerals (Fig. **8**).

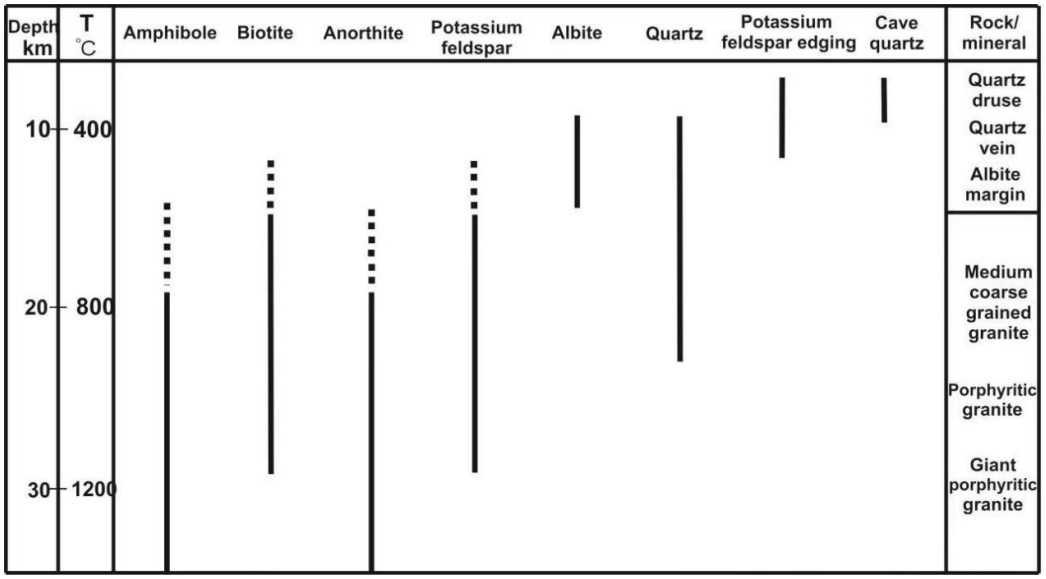

Figure 8: Sequence of mineral growth of Nansu rapakivi granite.

Secondly, according to the Ti content of ICP-MS in the laser denuded area of Single Zircon [32-34], the formation temperature corresponding to 27 age points is in the range of 641℃ ~ 695℃ (Fig. **9**), which is consistent with the variation range of 715℃~730℃ calculated according to zircon saturation [32-34]. Therefore, it is speculated that the formation depth is about 22km ~ 24km. Therefore, Nansu rapakivi granite was formed in a high-pressure medium, high-temperature environment with a depth of 23 km and a temperature of 670 ℃, consistent with the formation environment reflected by geochemistry.

In addition, the zircon ages of Nansu Rapakivi granite range from 113.6Ma to 122.6Ma (Fig. **9**), with an interval of 9Ma. Because of the limitations of the current experimental technical conditions, the ages of the most marginal and core parts can not be measured, so it is impossible to obtain the accurate age of the initial and termination growth of zircon particles. Under the condition of satisfying statistical significance, the maximum and minimum ages of single grain zircon can be used to approximately represent the initial and termination ages of minerals. It can be seen that the minerals in Nansu Rapakivi granite began to crystallize and grow from 123Ma to 113Ma. In the nearly 10Ma magmatic activity and diagenetic process, magmatism continues to occur and progress, but there are phased changes in the cooling rate of magma, making zircon and other minerals in changing environmental growth conditions. It can be seen from the data that in the period of 123Ma ~ 119Ma, the cooling rate of magma was faster, the growth environment of zircon was unstable, and the zircon mineral particles formed were less. From 119Ma to 116Ma, the magma cooling rate was slow, and the temperature was stable, which was conducive to the growth and development of zircon. From 116Ma to 113Ma, the cooling rate of magma tended to slow down, and zircon developed more and better (Fig. **9**).

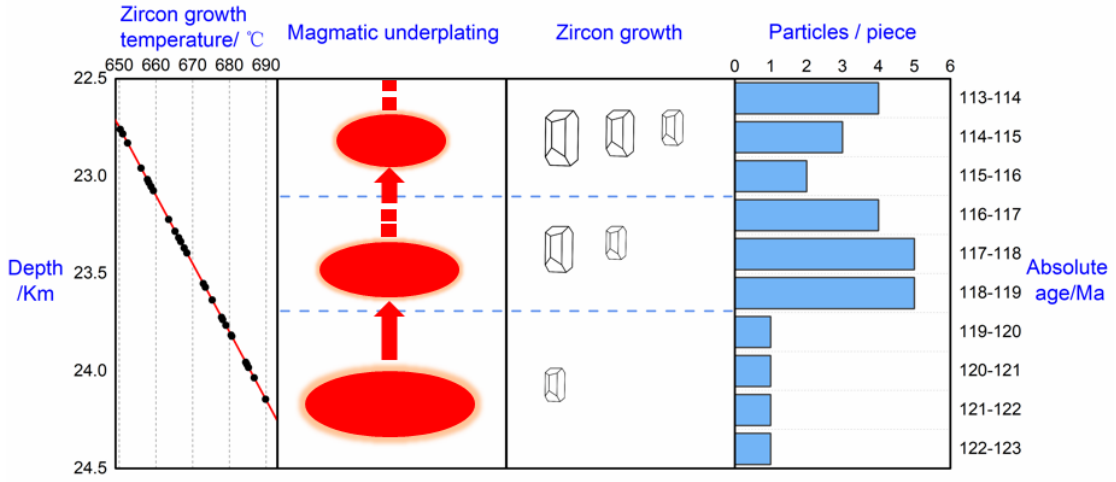

Figure 9: Simulation diagram and age histogram of magmatic zircon crystal growth.

6.2. Formation Mechanism of Nansu Rapakivi Granite

In Nansu large-scale rapakivi granite, large grain potassium feldspar is developed, the crystal form is intact, and the rapakivi is clear. The major elements show that it belongs to the quasi aluminous high potassium calc-alkaline potassic series granite. The combination of trace and rare earth elements shows that LREE enrichment, HREE loss, Nb, Ce, and Ti are negative anomalies, Pb is a positive anomaly, and Eu is a slightly negative anomaly. The average mass fraction of Nansu granite is la.3 ~ 4.08; Th/La mass fraction ratio is 0.28 ~ 0.53, with an average of 0.42. The above two ratios are higher than the average value of continental crust, indicating that Nansu granite has the characteristics of a crust source. It also conforms to the characteristics of I-type granite. According to the 1000Ga / Al-Zr diagram (Fig. **10**) and 1000Ga / Al-Y diagram (Fig. **10**), all points are located in the common area of I-type and S-type granite. According to the SiO_2-Zr diagram (Fig. **10**), all points are located in the area of I-type granite. According to the SiO_2-P_2O_5 diagram (Fig. **10**), SiO_2 and P_2O_5 of rock mass samples are negatively correlated, showing the evolution trend of I-type granite. It is not difficult to see from the above four diagrams that the Nansucun Rapakivi granite body is of I-type granite. The I-type granite has the addition of mantle-derived materials, and the rock mass is I-type granite, indicating that the Nansucun Rapakivi granite body may be affected by mantle-derived materials.

Sr content is higher than 400×10^{-6}μg/g, Yb content is lower than 2×10^{-6}μg/g, showing the characteristics of high Sr and low Yb [35], and there is no obvious negative Eu anomaly. The Sr / Yb ratio is high. It belongs to high-k Calc alkali adakite, which is speculated to be a typical adakite granite formed in a high-pressure environment [36]. Nb and Ti negative anomalies are obvious, suggesting that the magma source area has been mixed and metasomatized by crustal materials or subducted residual oceanic crust fluid [37]. Combined with the

geographical proximity to the Yangzi plate and Pacific plate, it is speculated that the formation of Nansu large-scale Rapakivi granite may be related to the subduction of the Mesozoic Pacific plate or the reactivation of the Yangtze plate.

Rb-(Y+ Nb) diagram shows that all sample points of Nansu Rapakivi granite fall into vag (volcanic arc granite) (Fig. **11**), indicating that its formation is related to subduction and is in the environment of the island arc. R1-R2 diagram and Rb/30-Hf-Ta×3 The triangular diagram also shows that the Nansu Rapakivi granite is the product of late collision or late orogeny (Fig. **12** and Fig. **13**), which is also consistent with the late orogenic characteristics that the rapakivi granite is mainly produced in the tensile environment. However, the particularity of the Nansu Rapakivi granite is that it is close to the area of the same collision period and has a transition type. It shows that the rapakivi granite was formed in the extensional environment of the island arc in the later stage of collision or orogeny.

This has the same genetic mechanism as the early Cretaceous granites in different areas of the Jiaobei uplift belt. According to the analysis of the tectonic background of the formation age, it may have received the subduction of the ancient Pacific plate, which triggered the partial melting of the thickened lower crust. At the same time, the magma was formed by the mixing of other magmas at the time of intrusion, and the early Cretaceous remelting granite was formed in the late collision and late orogeny.

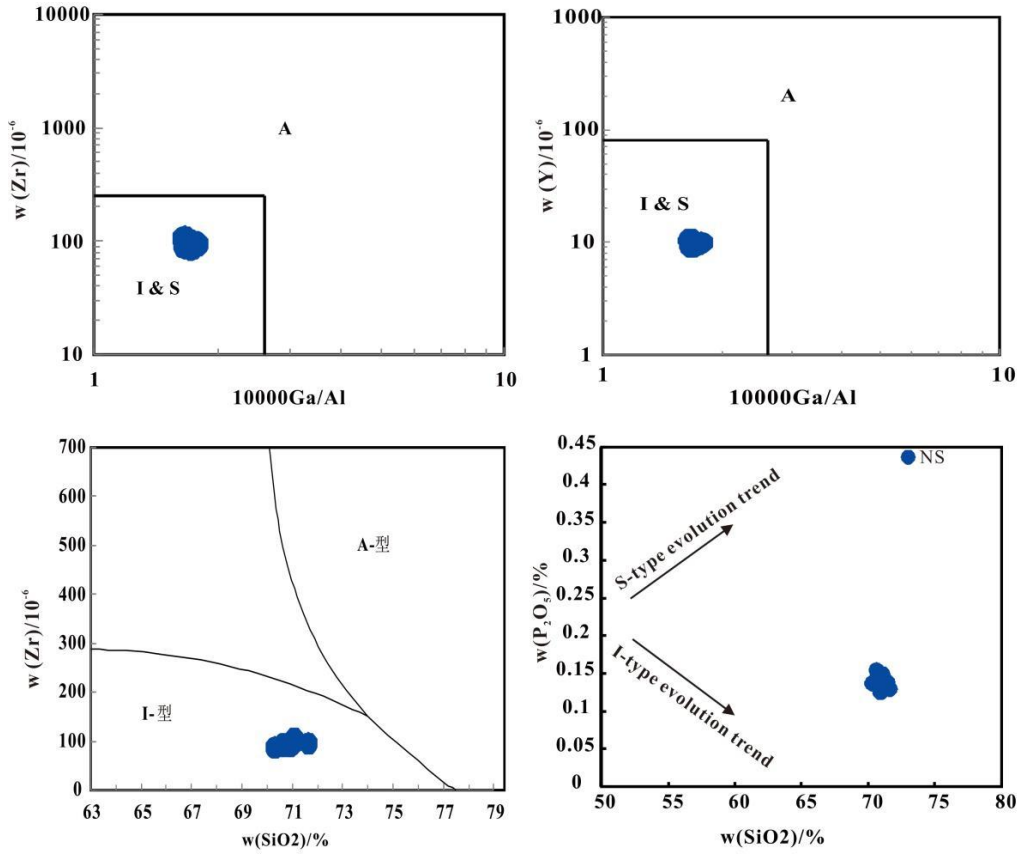

Figure 10: Granite type discrimination map group.

7. Conclusion

(1) Nansu rapakivi granite represents Mesozoic rapakivi granite widely distributed in Jiaobei uplift. Its 27 single grain zircon LA-ICP-MS U-Pb dating has a harmonic age of 116.5 ± 0.32Ma, and a weighted average age of 116.7 ± 0.89Ma, representing the crystallization age of Nansu large rapakivi granite and its formation age is early Cretaceous.

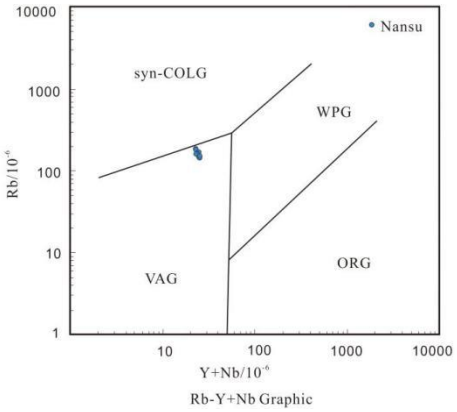

Figure 11: Rb - (Y + Nb) Diagram.

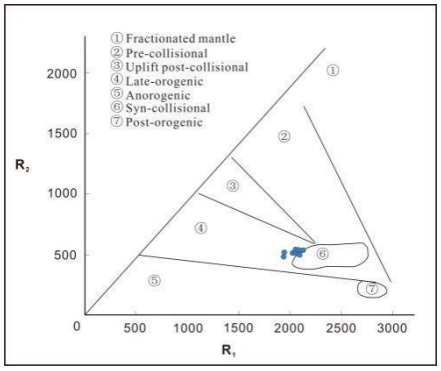

Figure 12: R1-R2 Diagram.

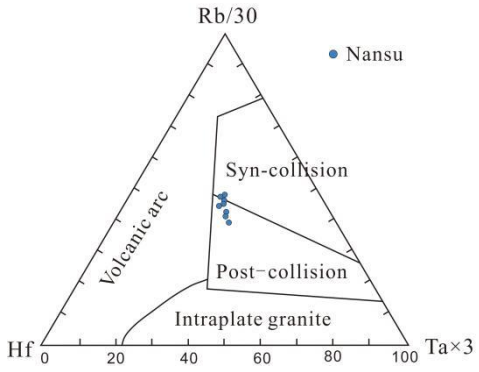

Figure 13: Rb / 30 -HF -Ta×3 Diagram.

(2) The crystallization sequence of mineral crystals in the outcrop rocks of Nansu Rapakivi granite, combined with the maximum and minimum ages of single grain zircon, it is considered that the minerals in Nansu Rapakivi granite began to crystallize and grow from 123Ma to 113Ma, and basically ended their development, experiencing three different cooling crystallization development histories.

(3) The SiO_2 content of Nansu large-scale rapakivi granite is 70.92%, and the average A / CNK is 0.883. It belongs to the quasi aluminous high potassium calc-alkaline potassic series. It is characterized by LREE enrichment, HREE loss, negative anomalies of Nb, Ce, and Ti, and positive anomalies of Pb. The average values of La / Nb and Th / La are 4.08 and 0.42, respectively, which are higher than the average value of continental crust, showing the characteristics of the crust source. It also conforms to the characteristics of I-type granite.

The average Sr content is 607×10^{-6}μg/g, and the average content of Yb is 0.96×10^{-6}μg/g. It has the characteristics of high Sr and low Yb, and it is a high potassium calc-alkaline Adake type granite formed under high

pressure, medium, and high-temperature environment of 23km and 667 ℃. It is speculated that the Nansu large-scale rapakivi granite was formed in the island arc environment, which is related to the subduction of the Mesozoic Pacific plate.

References

[1] Zhang L, Weinberg RF, Yang L-Q, Groves DI, Sai S-X, Matchan E, et al. Mesozoic Orogenic Gold Mineralization in the Jiaodong Peninsula, China: A Focused Event at 120 ± 2 Ma During Cooling of Pregold Granite Intrusions. Economic Geology 2020; 115(2): 415-441. https://doi.org/10.5382/econgeo.4716

[2] Li X-C, Fan H-R, Santosh M, Hu F-F, Yang K-F, Lan T-G. Hydrothermal alteration associated with Mesozoic granite-hosted gold mineralization at the Sanshandao deposit, Jiaodong Gold Province, China[J]. Ore Geology Reviews, 2013; 53. https://doi.org/10.1016/j.oregeorev.2013.01.020

[3] Fan HR, Zhai MG, Xie YH, Yang JH. Ore-forming fluids associated with granite-hosted gold mineralization at the Sanshandao deposit, Jiaodong gold province, China[J]. Mineralium Deposita, 2003; 38(6). https://doi.org/10.1007/s00126-003-0368-x

[4] Yang L-Q, Deng J, Goldfarb RJ, Zhang J, Gao B-F, Wang Z-L. 40 Ar/ 39 Ar geochronological constraints on the formation of the Dayingezhuang gold deposit: New implications for timing and duration of hydrothermal activity in the Jiaodong gold province, China[J]. Gondwana Research, 2014; 25(4). https://doi.org/10.1016/j.gr.2013.07.001

[5] Guangyuan C, Daisheng S, Shao YueGenetic mineralogy of accessory minerals of Kunyushan monzogranite in Jiaodong [J]Modern Geology, 1996; (02): 175-186.

[6] Willow. Study on the relationship between magmatic rocks and gold mineralization in jinyiling gold deposit, Zhaoyuan, Shandong [D]Central South University, 2014.

[7] Hong X. Zircon characteristics of Early Cretaceous granites in Jiaodong area and their constraints on gold mineralization [D]Chinese Academy of Geological Sciences, 2020.

[8] Yumin C, Qingdong Z, Zhifu S, Zhaokun W, Hongrui F, Fengli X, et al. Study on geochemical background of gold in Jiaodong [J]Gold science and technology, 2019; 27(06): 791-801.

[9] Yiduo Z, Junwei W, Zhaojun H, Jingjun Z. Geological characteristics and genetic analysis of Menlou mining area and peripheral gold deposits in Penglai City, Shandong Province [J]World nonferrous metals, 2016; (24): 50-51.

[10] Fancong M, Daisheng S, Shengrong L. Characteristics and mineralization of Cishan granite in Jiaodong [J]Deposit geology, 2001; (04): 394-401.

[11] Deming X, Jianming F, Xiqing C, Shunbo C, Liyan M, Kun Z, et al. Formation age, genesis and geological significance of dupanling rapakivi granite [J]Geotectonics and metallogeny, 2017; 41(03): 561-576.

[12] Baohang M. Genesis and tectonic significance of kangbaolujiaying giant porphyry granite in northern Hebei [D]Chengdu University of technology, 2016.

[13] Zheng Z. Characteristics and genesis of Qinling rapakivi granite [J]Knowledge window (Teacher Edition), 2017; (02): 32-33.

[14] Yizhen B. Magmatic crystallization genetic characteristics of K-feldspar giant phenocrysts in DAZHUANGKE granite body, Beijing [J]Journal of Hebei University of Geosciences, 1986; (02): 123-133.

[15] Haapala I, Rämö OT. Tectonic setting and origin of the Proterozoic rapakivi granites of southeastern Fennoscandia[J]. Transactions of the Royal Society of Edinburgh: Earth Sciences, 1992; 83(1-2). https://doi.org/10.1017/S0263593300007859

[16] Scandolara JE, Fuck RA, Dall'Agnol R, Dantas EL. Geochemistry and origin of the early Mesoproterozoic mangerite-charnockite-rapakivi granite association of the Serra da Providência suite and associated gabbros, central-eastern Rondônia, SW Amazonian Craton, Brazil[J]. Journal of South American Earth Sciences, 2013; 45. https://doi.org/10.1016/j.jsames.2013.03.003

[17] NengGao H, Xiaoxia W, Yangui S, Wenhuan S, Huanhuan C, Yunjie C. Geochemical characteristics, genesis and geological significance of Proterozoic Yingfeng Rapakivi Granite and its associated rocks in the northern margin of Qaidam [J]Geological review, 2007; (04): 460-472.

[18] Biao S. Isotopic geochronology, REE geochemical characteristics and genesis of Miyun rapakivi granite [a]Collected works of Institute of geology, Chinese Academy of Geological Sciences (25) [C]:Chinese Geological Society, 1993; 21.

[19] Liyakovicd VV. Rapakivi garite: problem of genesis and ore content.Geological Series 1991; (8): 51-65.

[20] Kovadi VB. Problem of anorthosite and rapakivi granite formations. Geological Joumal, 1989; (2): 48-54.

[21] Pavbovskiy EV. Problem of anorthosite and rapakivi garite, 1989; (5): 3-18.

[22] Xinxiang L, You D, Qiuling C, et al. Qinling Indosinian Shahewan Ordovician rapakivi granite and its dynamic significanceChinese science, Series D, 1996; 26(3): 244-248.

[23] Jianhua Y. Geochemical geology of the rapakivi granite suite in the Proterozoic rift trough in and around Beijing, 1990; 64(4): 322-336.

[24] Biao S. Isotopic geochronology, REE geochemistry and genesis of Miyun rapakivi graniteSee: Journal of Institute of geology, Chinese Academy of Geological Sciences (25 volumes), Beijing: Geological Publishing House, 1992; 137-156.

[25] Xuyang Z. Structural survey of Mesozoic granite and geological characteristics of typical gold deposits in Jiaodong [D]Chang'an University, 2018.

[26] Jianbo Z, Yongfei Z, Zifu Z. Zircon U-Pb age of Mesozoic Magmatic Rocks in Wulian, Shandong [J]Journal of geology of colleges and universities, 2003; (02): 185-194.

[27] Xiaoming L, Shan G, The fifth spring Rong, Yuan Honglin, Hu zhaochu20% of Single ZirconμSimultaneous determination of la-icp-msu-pb age and trace elements in the in situ micro region of M small spot bundle [J]Science Bulletin, 2007; (02): 228-235.

[28] Juan Z. Geochemical study of Mesozoic Magmatic Rocks in Sulu orogenic belt [D]. Hefei: University of science and technology of China, 2011.

[29] Boynton WV. Cosmochemistry of the Rare Earth Elements: Meteorite Studies[M]. one thousand nine hundred and eighty-four.

[30] Weaberbl. The origin of ocean island endember composistions:Traceelement and isotopic constrains [J].Earth And Planetary Science Letters, 1991; 104(2): 381-397. https://doi.org/10.1016/0012-821X(91)90217-6

[31] Geological Society, London, Special Publications 1989; 42: p. 313-345. https://doi.org/10.1144/GSL.SP.1989.042.01.19

[32] Watson EB, Wark DA, Thomas JB. Crystallization thermometers for zircon and rutile[J]. Contributions to Mineralogy & Petrology, 2006; 151(4): 413. https://doi.org/10.1007/s00410-006-0068-5

[33] Ferry JM, Watson EB. New thermodynamic models and revised calibrations for the Ti-in-zircon and Zr-in-rutile thermometers[J]. Contribut Mineral Petrol. 2007. https://doi.org/10.1007/s00410-007-0201-0

[34] Watson EB, Harrison TM, Watson EB, Harrison TM. Zircon saturation revisited: temperature and composition effects in a variety of crustal magma types. Earth Planet Sci Lett. 64, 295-304[J]. Earth and Planetary Science Letters, 1983; 64(2): 295-304. https://doi.org/10.1016/0012-821X(83)90211-X

[35] Xiaoyue G, Xianhua L, Zhigang C, Wuping L. Geochemical characteristics and genesis of Yanshanian high SR low Y-type intermediate acid igneous rocks in eastern China: constraints on crustal thickness in eastern China [J]Science Bulletin, 2002; (06): 474-480.

[36] Collins WJ, Beams SD, White AJR, Chappell BW. Nature and origin of A-type granites with particular reference to southeastern Australia[J]. Contributions to Mineralogy and Petrology,1982; 80(2). https://doi.org/10.1007/BF00374895

[37] Fitton JG, James D, Leeman WP. Basic magmatism associated with Late Cenozoic extension in the western United States: Compositional variations in space and time[J]. John Wiley & Sons, Ltd, 1991; 96(B8). https://doi.org/10.1029/91JB00372